Effects of Environmental Modulus and TGF-β1 Surface Concentration on Aortic Valvular Interstitial Cell Activation

Nicholas Alvey

Spring 2011

Advised by:
Dr. Kristi Anseth
Department of Chemical and Biological Engineering
Dr. Leslie Leinwand
Department of Molecular, Cellular, and Developmental Biology

University of Colorado at Boulder

ABSTRACT

Valvular Interstitial Cells (VICs) are the predominant cell population of mammalian heart valves. When the valve is damaged, VICs become activated to a myofibroblastic state and secrete a variety of matrix molecules in order to repair the valve structure. However, in aortic valve stenosis, the VICs differentiate to an osteoblastic state. This phenotype ultimately calcifies the valve resulting in valvular stenosis, which eventually requires valve transplantation for prolonged survival. It has been previously shown that this activation is modulated separately by the cytokine transforming growth factor beta-1 (TGF-β1) as well as mechanical properties of the extracellular microenvironment, notably the environmental modulus. In this investigation, hydrogels of soft and stiff moduli with varying surface concentrations of covalently tethered TGF-β1 were constructed in order to assess the effect of varying both environmental modulus and TGF-β1 concentration. On softer substrates, VICs exhibited a rounded morphology and clustered together. As a result, there was little variation in activation or cell density between different TGF-β1 conditions. On stiffer substrates, VICs exhibited a more spread morphology and higher cell density on all conditions compared to soft conditions. In response to varying levels of TGF-β1 surface concentrations, VICs increased in activation from 0 to 16 ng/cm^2 TGF-β1, but then significantly decreased in activation from 16 to 32 ng/cm^2. VICs were also seen to form nodules on 32 and 64 ng/cm^2 TGF-β1 conditions but not on 0 and 16 ng/cm^2 conditions. These results suggest there is a TGF-β1 concentration threshold between the 16 and 32 ng/cm^2 below which VICs remain activated and in a myofibroblastic state and above which VICs progress to a disease-like state. However, further cellular characterizations are needed to confirm these conclusions.

TABLE OF CONTENTS

LIST OF FIGURES

Introduction

Aortic Valve Native Biology

The aortic valve serves as the primary gate through which the heart pumps oxygenated blood into the systemic circulatory system of the body. Through this process, the valve undergoes a variety of mechanical stresses when opening to allow the ejection of blood from the left ventricle and closing to prevent backflow of blood from the aorta. It has been estimated that pressures experienced by the leaflet are around 50 kPa during systole and 500 kPa during diastole (Thubrikar et al., 1980). Thus, valve histology and biology are optimized to handle these fluctuating pressure conditions. Histologically, the valve can be divided into three layers (from the aortic side to the ventricular side): the fibrosa, spongiosa, and ventricularis (Butcher et al., 2011). The fibrosa is primarily composed of collagen bundles arranged in a circular array throughout the valve; these bundles bear the most pressure during the diastolic phase (Thubrikar et al., 1980). The spongiosa consists mostly of glycosaminoglycans (GAGs) as well as a small, heterogeneous population of other fibrous proteins (Butcher et al., 2011). Finally, the ventricularis is comprised mainly of elastin, allowing the valve to flex considerably between systole and diastole. It is important to note that the valve is avascular, and therefore receives most of its nutrients via hemodynamic diffusion.

There are two cell types that occupy most of the valve structure (Butcher et al., 2011). Valvular endothelial cells form a monolayer around the outside of the valve and facilitate diffusion of nutrients from the blood flow. Valvular interstitial cells (VICs) compose the primary cell type within the valve, and while they are a heterogeneous population, they generally exhibit a fibroblastic phenotype (Butcher et al., 2011; Liu et al., 2007). The VICs' primary function within the valve is to remodel the extracellular environment in response to varying stresses.

However, these two cell populations are not isolated from each other and have been show to actively communicate in directing valve remodeling (El-Hamamsy et al., 2008).

When the valve becomes damaged through any number of injury mechanisms, VICs become activated and differentiate from a quiescent state to a myofibroblastic phenotype, most likely through an immunoresponse similar to general wound healing (Liu et al., 2007). Activated VICs express heightened levels of α-smooth muscle actin (αSMA), the primary indicator of myofibroblast phenotype (Hinz, 2007; Liu et al., 2007). The cells will also organize αSMA into striated stress fibers throughout their cytoskeleton, an easily visible phenotype through immunostaining (Darby et al., 1990; Liu et al.). In a wound response mechanism, VIC activation is most likely driven by the presence of transforming growth factor β1 (TGF-β1), which has been shown to activate VICs *in vitro* in multiple studies (Mohler et al., 1999; Jian et al., 2003; Walker et al., 2004; Cushing et al., 2005; Benton et al., 2010). The cyclic strain of the valve opening and closing as well as the environmental modulus can also drive VIC activation during the wound healing process (Kloxin et al., 2010; Ferdous et al., 2011). Once the wound is repaired, VICs revert back to their quiescent state or apoptose (Desmouliere et al, 1997); thus, quiescent and activated VICs are in a dynamic equilibrium influenced by the presence or lack of specific cytokines as well as the environmental mechanical strain (Liu et al., 2007; Kloxin et al., 2010; Ferdous et al., 2011).

Molecular Pathology of Aortic Valve Disease

There are a variety of molecular pathologies associated with aortic valve disease and its progression. This condition can range from mild leaflet thickening, termed aortic valve sclerosis, to severe leaflet thickening, calcification, and significant functional decrease, termed aortic valve

stenosis (Freeman, 2005). Usually, one of the first processes to occur within a diseased valve is neoangiogenesis. Then, an immune response of infiltrating macrophages and T-lymphocytes in response to pro-inflammatory cytokines such as interleukin-1β and TGF-β1 occurs (Kaden et al., 2003; Jian et al., 2003). Also, localized lipid accumulation has been shown to occur throughout diseased valves (Otto et al., 1994). At these lipid foci, localized calcification has also been reported (Warren et al., 1997). Differential genetic factors contributing to this process have also been identified. Among others, chondromodulin I expression is downregulated in diseased valves, relative to its levels in non-diseased valves (Yoshioka et al., 2006). Because of chondromodulin I's antiangiogenic properties, it is hypothesized that this protein is responsible for maintaining aortic valve avascularity, thereby preventing the progression to a diseased phenotype. Proteins found to be upregulated in calcific valves include BMPs, osteopontin, collagen I, and osteocalcin (Freeman, 2005; Liu et al., 2007).

VICs also play a crucial role in the pathological progression of aortic valve disease. While they differentiate to an activated, myofibroblast phenotype during valve wound repair as well as pathological conditions, they have also been reported to progress to an osteoblastic phenotype, forming calcific nodules both *in vitro* and *in vivo* (Mohler et al., 1999). These nodules are dependent upon alkaline phosphatase activity (Mathieu et al., 2005) and accelerate in their development with the addition of TGF-β1 (Jian et al., 2003). After contracting into nodules and upregulating the previously listed proteins associated with calcification, many of the VICs undergo apoptosis (Jian et al., 2003). The formation of nodules and calcium production have severe effects on valve function. As the valve becomes stiffer due calcium deposits, its ability to close and prevent regurgitation of blood becomes hampered. This can eventually lead to heart failure and requires valve replacement (Butcher et al., 2011).

Use of Tethered Growth Factors to Influence Cell Behavior

In vivo, signaling proteins are tethered within the extracellular matrix (ECM) via interactions with charged molecules within the ECM, such as proteoglycans (Lutolf et al., 2009). While soluble growth factors play an important role in controlling cell behavior, many investigations have been published that show the beneficial effects of tethered growth factors over soluble growth factors. For example, tethered epidermal growth factor (EGF) is superior in causing the spread of mesenchymal stem cells when compared to soluble dosage (Fan et al., 2007). Also, when presented with tethered versus soluble fibroblast growth factor 2 (FGF2), embryonic stem cells had increased proliferation (Nur-E-Kamal et al., 2008).

TGF-β1 has also been successfully tethered into biomaterial matrices and shown to remain bioactive. Specifically, TGF-β1, covalently attached to a PEG monomer, was tethered into a PEG-diacrylate hydrogel and shown to increase matrix production of smooth muscle cells relative to soluble delivery (Mann et al., 2000). TGF-β1 immobilized to the surface of a polymer substrate was able to suppress the progression of chondrocytes down an osteogenic lineage (Chou et al., 2005). Finally, TGF-β1 adsorption to Ti6Al4V substrates, a material often used in orthopedic implants, was able to increase pro-collagen mRNA levels in osteoblast culture over a period of 3 weeks (Fischer, 2003). VICs have also been shown to be activated by TGF-β1 sequestered to heparin moieties in biomaterials, where it was concluded that the heparin molecules stabilized TGF-β1 within the microenvironment for cellular activation (Cushing et al., 2005).

Environmental Stiffness Effects on Cell Behavior

Environmental stiffness plays an important role in determining cell behavior. Generally, transmembrane cell adhesion receptors, such as integrins, have a tug-of-war interaction with the surrounding matrix. Integrins and the actin-myosin cytoskeleton will exert force on the ECM, which, in turn, resists that force (Bershadsky, 2006; Ingber, 2006). Stiffer matrices usually result in the clustering of integrins, thereby increasing the number of focal adhesion sites and the tension on the intracellular cytoskeleton, resulting in a more spread cellular phenotype (Wells, 2008). However, cells cultured on softer substrates have fewer focal adhesions, resulting in a rounded phenotype more prone to apoptosis.

Recently, many reports have been published linking environmental stiffness directly to cell differentiation. One such study showed that matrix stiffness could direct the differentiation of human mesenchymal stem cells (hMSCs) down several unique lineages (Engler et al., 2006). Specifically, polyacrylamide hydrogels were made with moduli similar to the physiological moduli of brain, muscle, and bone tissue. hMSCs seeded on these different hydrogels then differentiated to the corresponding tissue type. Furthermore, Gilbert et al. in 2010 cultured muscle stem cells (MuSCs) on substrates that mimicked the modulus of muscle and reported sustained stem cell phenotype in culture, which had not been previously possible on traditional tissue culture polystyrene (TCPS) plastic. Finally, it has been shown in multiple reports that fibroblasts cultured on stiffer substrates undergo a greater degree of myofibroblast differentiation than on softer substrates (Wells, 2008; Li, 2007; Tomasek, 2002).

Specifically in VIC cultures, studies have been published showing the effects of matrix stiffness on VIC behavior. Kloxin et al. observed VIC differentiation to a myofibroblast phenotype at stiff modulus (~32 kPa), but showed cell deactivation when the modulus of the

matrix was lowered, via photochemical methods (2008). In the same study, a modulus gradient was fabricated throughout a single hydrogel, concluding that ~15 kPa was a threshold modulus, above which VICs become activated to a myofibroblast phenotype and below which they remain quiescent. Another study exposed VICs to cyclic stressing and observed increased MMP-2 production, calcium content, and alkaline phosphatase activity compared to a negative control (Ferdous et al., 2011). From these studies, it is clear that this cell population, like many others, is responsive to environmental stiffness, and such a parameter should be considered when fabricating VIC biomaterial platforms for culture and experimentation.

Central Question

While effects of environmental modulus as well as TGF-β1 on VIC behavior have been individually characterized, the effects of concurrently varying both of these conditions have yet to be tested. In this investigation, hydrogels with varying surface concentrations of covalently tethered TGF-β1 and various stiffness were constructed. VICs were then seeded on these constructs, and their adhesion capability and activation to the myofibroblast phenotype were assessed.

Methods

PEG-Norbornene synthesis

Description of PEG-Norbornene synthesis has been previously described elsewhere (Fairbanks et al., 2009). Briefly, Norbornene-functionalized PEG was prepared by the addition of norbornene acid via the symmetric anhydride N,N'-dicyclohexylcarbodiimide (DCC; Sigma) coupling. 4-arm PEG, MW 10,000 (JenKemUSA), was dissolved in anhydrous dichloromethane (DCM) with pyridine and 4-(dimethylamino)pyridine (DMAP; Sigma). In a separate reaction vessel, DCC was reacted with 5-norbornene-2-carboxylic acid (Sigma) to form the dinorbornene carboxyclic acid anhydride. The anhydride was allowed to stir for 15 minutes, with subsequent addition of the 4-arm PEG, pyridine, and DMAP solution and allowed to stir overnight. This mixture was filtered and the filtrate precipitated in ice-cold diethyl ether. The product was desiccated overnight and purified using soclet extraction into ethyl ether.

Preparation of Thiolated Coverslips

12-mm cover slips (Warner Instruments) were immersed in piranha solution (15% hydrogen peroxide in 5 M sulfuric acid) for 1 hour at room temperature. Cover slips were then removed and briefly washed in diH_2O and acetone before being air-dried. Slips were placed in a sealed chamber with 60 μL of 3-mercaptopropyl trimethoxysilane (Sigma) for 3 hours at 60^{o} C. Cover slips were immediately removed from the chamber and stored at -20^{o}C until further use.

Hydrogel Preparation and Modulus Quantification

Hydrogels were prepared via step growth free radical polymerization of 4-arm poly (ethylene glycol) (PEG) norbornene and cross-linked with dithiothreitol (DTT; Sigma). PEG-norbornene

(10 mM) was combined with 194 mM DTT (3:2 alkene:thiol), with 1 mM lithium phenyl-2,4,6-trimethylbenzoylphosphinate photoinitiator (LAP; Fairbanks et al., 2009) and 1 mM CRGDS. Monomer solution (35 μL) was transferred into 12-mm diameter molds in contact with a thiolated glass cover slip. Solutions were irradiated with 365 nm light source (Omnicure) at an intensity of 10 mW/cm^2 for 4 minutes. The resulting hydrogels were swollen in PBS at 4^{o}C for at least 24 hours. Young's modulus was controlled by varying the weight percent of PEG-norbornene in monomer solutions, and swollen modulus measured using a rheometer (TA Ares).

TGF-β1Thiolation

Traut's reagent (2-Iminothiolane; ThermoScientific) was reconstituted in PBS at 140 μM with 50 mM EDTA. TGF-β1 (Peprotech) was reconstituted in Traut's solution at 50 μg/mL and incubated at room temperature for approximately one hour. After incubation, BSA (at 10% w/v) was added to the reaction solution, and thiolated TGF- β1 was aliquoted and stored at -20^{o}C until further use.

Surface Bioactivation

Preformed hydrogels were incubated for greater than 30 minutes in 0.05% I2959 photoinitiator (Ciba Specialty Chemicals). Thirty μL of varying dilutions of thiolated TGF-β1 were then pipetted onto the polymer surface, and hydrogels were exposed to 365 nm UV light at 10 mW/cm^2 for 5 minutes. The hydrogels were subsequently washed 2 times for at least 10 minutes in PBS at room temperature, then washed overnight at 4^{o}C in PBS.

TGF-β1 ELISA Quantification

TGF-β1 conjugated gels were characterized using a modified enzyme linked immunosorbent assay (ELISA) (Hume & Anseth, 2010). Hydrogels were incubated in 5 wt% BSA solution for 4 hours at room temperature to block non-specific antibody binding. Mouse anti-human TGF-β1 primary antibody (Peprotech) in 5 wt% bovine serum albumin (BSA; Sigma) was added to each sample and allowed to incubate at room temperature for 1 hour. After washing in 0.05% Tween-20 supplemented PBS (PBST; Sigma), gels were incubated in goat anti-mouse horseradish peroxidase (eBioscience) at room temperature for 30 minutes. After PBST washes, gels were incubated with 3,3',5,5'-tetramethylbenzidine (TMB; Sigma). After appropriate color development, enzymatic reaction was terminated with 2 M H_2SO_4. and solutions analyzed at 450 nm on a Wallac Victor^2 1420 Multilabel Counter plate reader (PerkinElmer).

Bioactivation Assessment

Bioactivation of TGF-β1 was assessed with the PE-25 cell line graciously donated by Professor Xuedong Liu. The cell line is derived from the mink lung epithelial cells and stably transfected with a luciferase reporter gene driven by the plasminogen activator inhibitor-1 gene promoter, a gene that is known to be activated by TGF-β1 signaling (Hua et al., 1998; Clark et al., 2009). The PE-25s were cultured on TCPS plates in Dulbecco's modified Eagle media supplemented with 10% fetal bovine serum (FBS), penicillin/streptomycin (200 U/mL), and fungizone (1.0 μg/mL), maintained in a humid incubator at 37^{o}C and 5% CO_2, and expanded via successive trypsinization. In assessing thiolated TGF-β1 activity, cells were added to a TCPS plate at 250,000 cells/cm^2 and allowed to attach to the plate for 4 hours at 37^{o}C and 5% CO_2. 5 ng/mL of TGF-β1 diluted in high glucose Dulbecco's modified Eagle media supplemented with

penicillin/streptomycin (200 U/mL), and fungizone (1.0 μg/mL) was added to the cells and allowed to incubate at 37°C and 5% CO_2 for approximately 20 hours. After incubation, the TGF-β1 solution was aspirated off the plate. In assessing bioactivation of hydrogel surfaces, PE-25 cells were added to the hydrogel surface at 250,000 cells/cm^2 and allowed to incubate at 37°C and 5% CO_2 for approximately 20 hours. After incubation, the hydrogels were carefully removed and placed in a fresh plate. In both cases, Glo Lysis Buffer (Promega) was placed in each well for 10 minutes after which the plate was stored at -80°C for at least one hour. The plates were then thawed, and the cell lysate was centrifuged at 15,000 rpm for 10 minutes. The resultant supernatant was mixed at a volumetric 2:1 ratio with luciferin ((4*S*)-2-(6-hydroxy-1,3-benzothiazol-2-yl)-4,5-dihydrothiazole-4-carboxylic acid) in a 96-well white plate, and luminescence was immediately read on a Wallac Victor^2 1420 Multilabel Counter plate reader (PerkinElmer).

VICs Preparation

VICs were isolated from the aortic valves of porcine hearts obtained, on ice, within 24 hours of sacrifice of the animal from Hormel Inc. (Austin, MN). The cusps of the aortic valves were surgically removed, rinsed in Earl's Balanced Salt Solution (EBSS), and subjected to sequential collagenase digestion. The VICs were cultured on TCPS plates in M199 media supplemented with 15% FBS, penicillin/streptomycin (200 U/mL), and fungizone (1.0 μg/mL). They were maintained in a humid incubator at 37°C and 5% CO_2 and expanded by successive trypsanization. VICs were seeded on surface-functionalized hydrogels at a density of 30,000 cells/cm^2 in M199 media supplemented with 1% FBS, penicillin/streptomycin (200 U/mL), and fungizone (1.0 μg/mL), and allowed to incubate for 3 days. Activation of the cells was

characterized by immunostaining for the myofibroblast marker alpha smooth muscle actin (αSMA) and computing the ratio of cells with readily apparent stress fiber formation within the cytoskeleton to the total number cells within the viewing area.

Immunostaining

Hydrogels were fixed in 4% paraformaldehyde solution at room temperature for 15 minutes and then washed in PBS overnight at 4^{o}C while rocking. After washing, the cells were permeabilized in 0.1% Triton-X (FischerBiotech) for 30 minutes and then blocked from non-specific antibody staining in 5 wt% BSA for 1 hour at room temperature. Samples were incubated in 1:100 dilution of mouse anti-αSMA (Abcam) primary antibody diluted into 1 wt% BSA and 0.05% Tween-20 (Sigma) overnight at 4^{o}C while rocking. Samples were washed in PBST and incubated in 1:400 dilution of goat anti-mouse secondary antibody conjugated to an Alexa®488 fluorophore (Invitrogen) for 1 hour at room temperature. After another wash with 0.05% PBST, the samples were incubated with DAPI nuclear staining and imaged on a Nikon TE 2000 epi-fluorescence microscope within 24 hours.

Results

Surface Activated Hydrogel Characterization

In this study, TGF-β1 was covalently conjugated to the top face of hydrogels to produce a bioactive surface. In order for the covalent conjugation to occur, TGF-β1 was initially thiolated in order to utilize the thiol-ene chemistry capabilities of PEG-norbornene hydrogels. This was accomplished by incubating lyophilized TGF-β1 with a large molar excess of Traut's reagent (2-iminothiolane). The bioactivity of the thiolated TGF-β1 was then assessed against non-thiolated TGF-β1 via a luciferase reporter gene assay (Fig. 1). 5 ng/mL of thiolated and non-thiolated

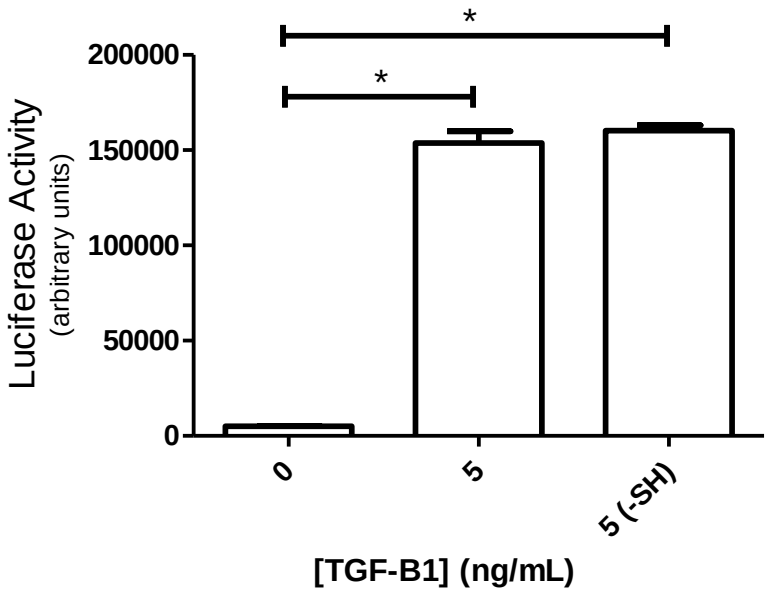

Figure 1 – Luciferase activity from transfected PE-25 cells exposed to 0 and 5 ng/mL soluble TGF-β1 (left and center columns, respectively) and 5 ng/mL soluble thiolated TGF-β1 (right column). Cells were seeded at 250,000 cells/cm^2 in TCPS plates and exposed to the respective conditions for 20 hours. * denotes $p < 0.0001$. Each condition is n=5.

TGF-β1 were incubated for 20 hours with PE-25 cells. PE-25s are immortalized fibroblasts derived from the mink lung epithelium and transfected with the firefly luciferase gene driven by the plasminogen activator inhibitor-1 promoter, which is known to be activated during TGF-β1 signaling (Hua et al., 1998; Clark et al., 2009). PE-25s exhibited similar luciferase activity in the

presence of both thiolated and non-thiolated TGF-β1, and these activities were significantly greater ($p < 0.0001$) than the luciferase response to no TGF-β1.

Thiolated TGF-β1 was then conjugated to the surface of hydrogels via photopolymerization. Hydrogels were soaked for at least 30 minutes prior to the polymerization reaction in an I2959 photoinitiator solution, the appropriate TGF-β1 concentration pipetted onto the top of the polymer surface, and exposed to 365 nm ultraviolet light. To confirm the presence of TGF-β1 on the hydrogels, a modified ELISA technique was employed (Hume & Anseth, 2010). The surface concentration was estimated as the total mass of TGF-β1 added divided by the surface area of the hydrogel's top face. Hydrogels with TGF-β1 surface concentrations increasing in a linear fashion exhibited a linear ELISA response (Fig. 2), thereby both confirming the presence of TGF-β1 on the hydrogel as well as the ability to control the amount of TGF-β1 that is conjugated to the hydrogel.

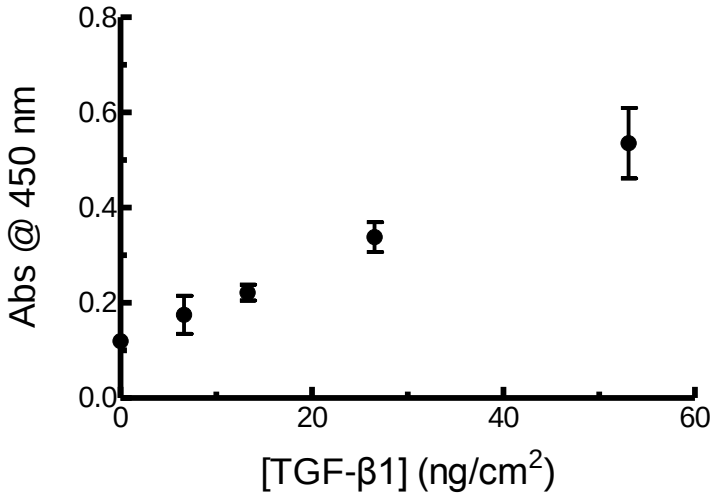

Figure 2 – Immunodetection of TGF-β1 on bioactive hydrogel surfaces. Hydrogels at ~11 kPa were conjugated with 0, 6.64, 13.27, 26.55, and 53.09 ng/cm^2, and TGF-β1 surface density was determined by a modified ELISA. Error bars represent standard error of the mean, and each condition had a n=5.

Furthermore, while the ELISA technique confirms the presence of TGF-β1, it does not necessarily confirm the bioactivity of the growth factor, only the availability of binding epitopes

for detection antibodies. In order to assess bioactivity, the PE-25 assay was once again used. PE-25 cells were seeded on the surface of hydrogels conjugated with 0, 8, 21, 42, and 84 ng/cm^2 TGF-β1 and allowed to incubate for 20 hours. Similar to the ELISA results in Figure 2, the luciferase activity from these hydrogels exhibited a linear response, thereby confirming both the presence of bioactive TGF-β1 as well as the ability to produce an increasing cellular response to increasing TGF-β1 levels (Fig. 3).

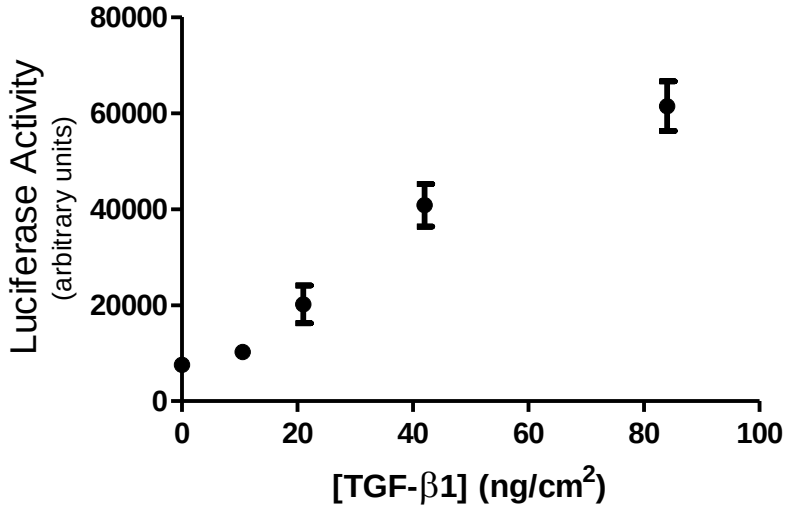

Figure 3 – Luciferase activity from transfected PE-25 cells seeded on top of hydrogels with TGF-β1 bioactive surfaces. Hydrogels at ~11 kPa were conjugated with 0, 8, 21, 42, and 84 ng/cm^2 TGF-β1, seeded with PE-25 cells at 250,000 cells/cm^2, and allowed to incubate for 20 hours. Errors bars represent standard error of the mean, and each condition was done in triplicate.

In order to investigate VIC response to varying environmental moduli, hydrogels were constructed with different weight percent monomer solutions. Hydrogels of 5%, 10%, and 20% PEG-norbornene monomer solutions were polymerized and allowed to swell in PBS for at least 24 hours before the modulus was measured via rheometry. The 5%, 10%, and 20% monomer solutions had average Young's moduli of 4.1, 11.6, and 21.3 kPa, respectively (Fig. 4). VICs are known to become activated and exhibit a myofibroblast phenotype when exposed to a substrate with Young's modulus greater than 15 kPa (Kloxin et al., 2010). Thus, from the distribution of

Young's moduli obtained via augmenting the monomer weight percent, biomaterials can be fabricated to expose VICs to both soft (<15 kPa) substrates and activating, stiff (>15 kPa) substrates.

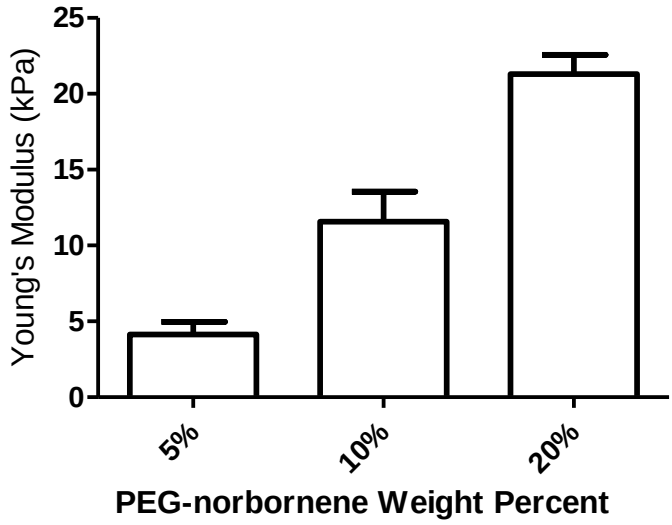

Figure 4 – Swollen Young's modulus of varying weight percent PEG-Norbornene hydrogels evaluated via rheometry. Hydrogels were polymerized with 5%, 10%, and 20% 4-arm PEG-Norbornene monomer solutions. Error bars represent standard error of the mean, and each condition was done in quadricate.

Finally, in order to promote VIC adhesion to hydrogel surfaces, hydrogels were constructed with a short pendant peptide C**RGDS**. The bolded portion of the polypeptide sequence is the integrin-binding motif derived from the extracellular matrix protein fibronectin (Ruoslahti, 2006). The extra cysteine moiety was added in order to use the primary thiol side chain in a thiol-ene conjugation reaction, thus covalently tethering the short peptide into the hydrogel matrix. In Figure 5, VICs were seeded on hydrogels with 1 mM and 2 mM C**RGDS** incorporated into the matrix (5A and 5B, respectively) and compared to VICs seeded on tissue culture treated polystyrene plates (TCPS, 5C). Morphologically, VICs seeded on both 1 mM and 2 mM C**RGDS** supplemented hydrogels did not exhibit any difference from cells seeded on TCPS plates. Similarly, VICs seeded on 1 mM and 2 mM C**RGDS** supplemented hydrogels did

not visually vary in density when compared with VICs seeded on TCPS plates. Thus, for the remainder of the study, 1 mM C**RGDS** supplemented hydrogels were used.

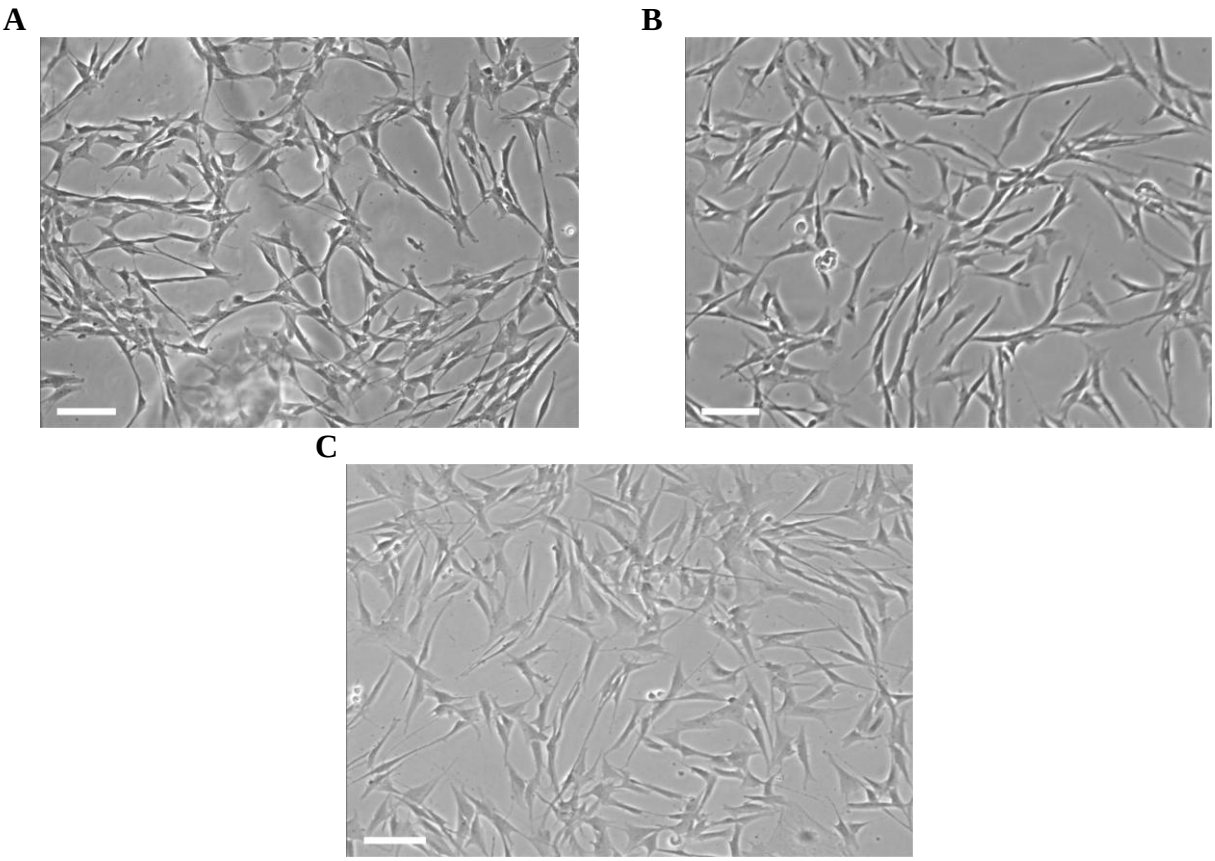

Figure 5 – Bright-field images of VICs seeded on 20 wt% PEG-Norbornene hydrogels with A) 1 mM CRGDS incorporated, B) 2 mM CRGDS, and C) on a TCPS plate. VICs were seeded at 35,000 cells/cm^2 and allowed to attach over a 24-hour period. Scale bar represents 100 μm.

VIC Adhesion and Activation

To assess VIC behavioral response to varying combinations of environmental moduli and TGF-β1 surface densities, soft and stiff hydrogels of 4 kPa and 21 kPa were constructed in order to evaluate VIC behavior below and above (respectively) the 15 kPa modulus activation threshold (Kloxin et al., 2010). After hydrogels were polymerized, 0, 16, 32, and 64 ng/cm^2 of thiolated TGF-β1 was then conjugated to the top face of the hydrogel. VICs were seeded on these hydrogels and allowed to incubate for 72 hours before being fixed and imaged. The

samples were stained for the myofibroblast marker α-smooth muscle actin (αSMA) (Darby et al., 1990; Liu et al., 2007) and DAPI nuclear stain. Percent activation was then calculated by observing the number of VICs with at least one αSMA-positive stress fiber, an indicator of myofibroblast phenotype (Hinz, 2007), divided by the total number of DAPI-positive cells in the frame. On average, approximately 96 cells were counted per condition.

Activation of 4 kPa hydrogels is shown in Figure 6. VIC activation seems to increase slightly overall when TGF-β1 surface concentration was increased. There is also a slight drop in VIC activation from the 16 ng/cm^2 to the 32 ng/cm^2 condition. However, these variations are not statistically significant, and there was relatively wide variability in VIC activation from replicate to replicate within each condition. Activation on the 21 kPa hydrogels is shown in Figure 7. VIC activation increases from 0 ng/cm^2 to 16 ng/cm^2 and then sharply drops from the 16 ng/cm^2 condition to the 32 ng/cm^2 condition ($p < 0.01$).

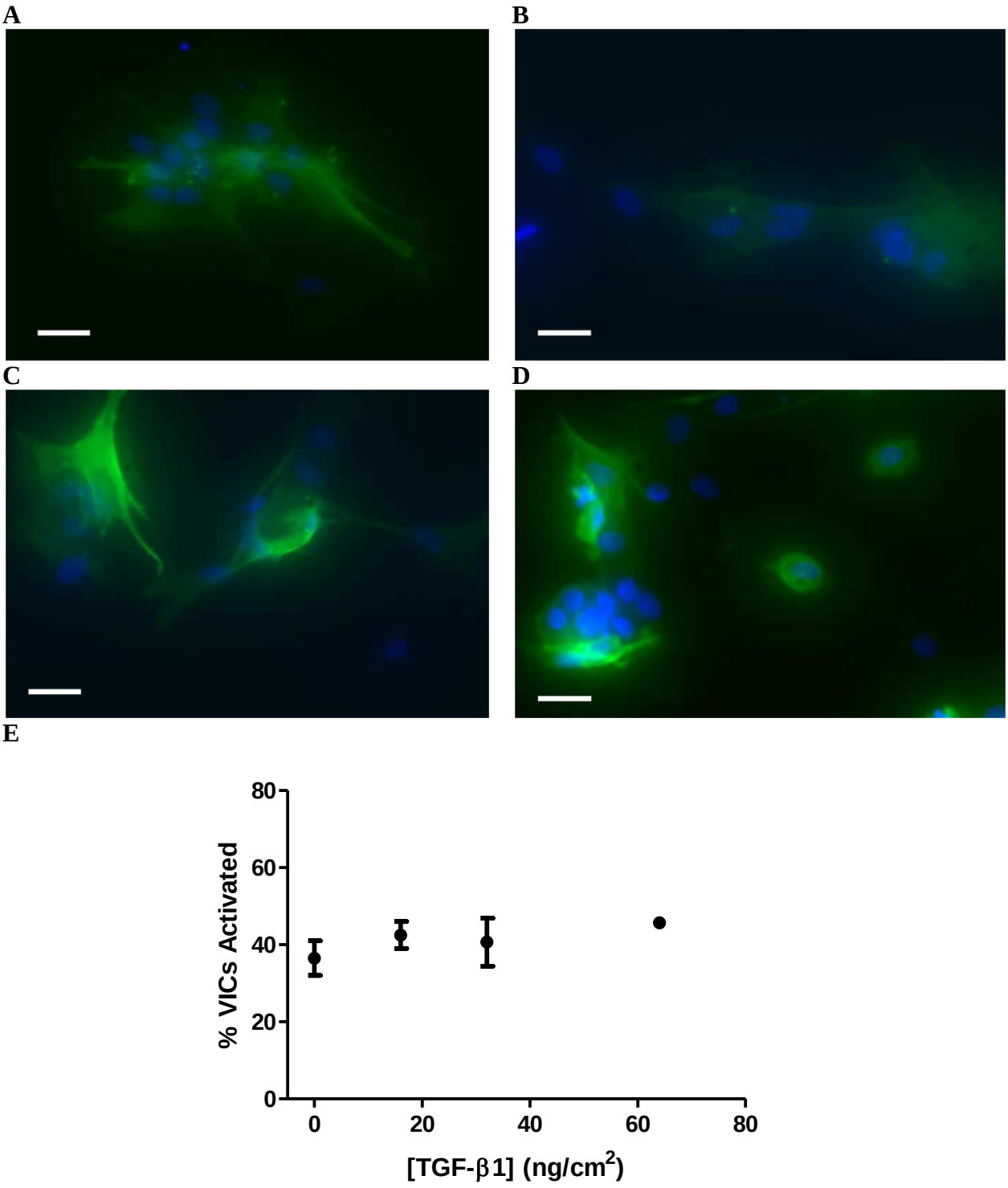

Figure 6 – 4 kPa hydrogels conjugated with A) 64 ng/cm^2, B) 32 ng/cm^2, C) 16 ng/cm^2, and D) 0 ng/cm^2 TGF-β1. VICs were seeded at 30,000 cells/cm^2 and allowed to incubate for 72 hours at which point they were fixed and stained for αSMA (green) and DAPI (blue). Scale bar represents 50 μm. E) Percent activation was calculated as cells with at least one αSMA stress fiber divided by total number of cells. Error bars represent standard error of the mean, and each condition was done in triplicate.

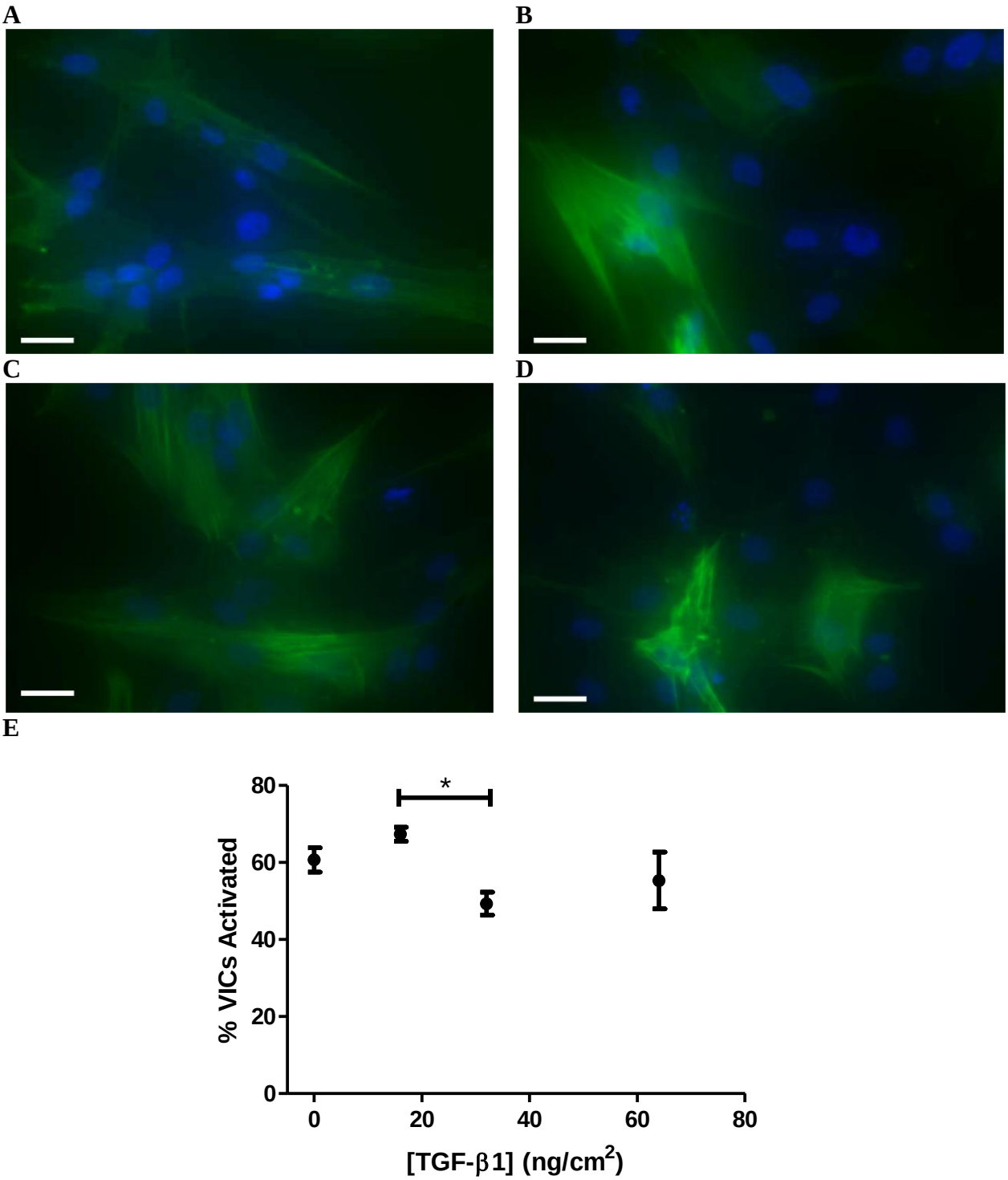

Figure 7 – 21 kPa hydrogels conjugated with A) 64 ng/cm^2, B) 32 ng/cm^2, C) 16 ng/cm^2, and D) 0 ng/cm^2 TGF-β1. VICs were seeded at 30,000 cells/cm^2 and allowed to incubate for 72 hours at which point they were fixed and stained for αSMA (green) and DAPI (blue). Scale bar represents 50 μm. E) Percent activation was calculated as in Figure 6. Error bars represent standard error of the mean, and each condition was done in triplicate. * denotes $p < 0.01$.

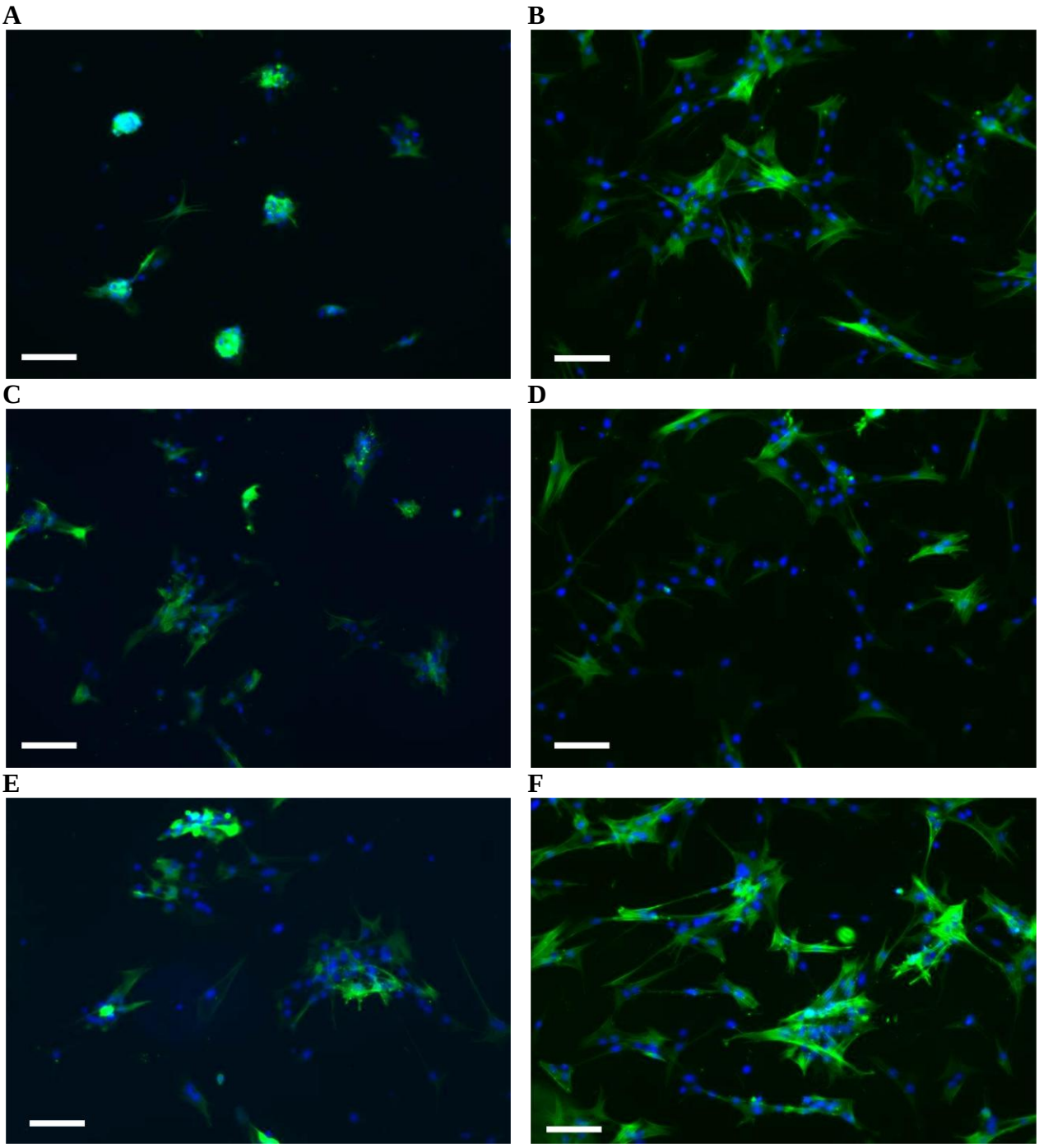
A
B
C
D
E
F

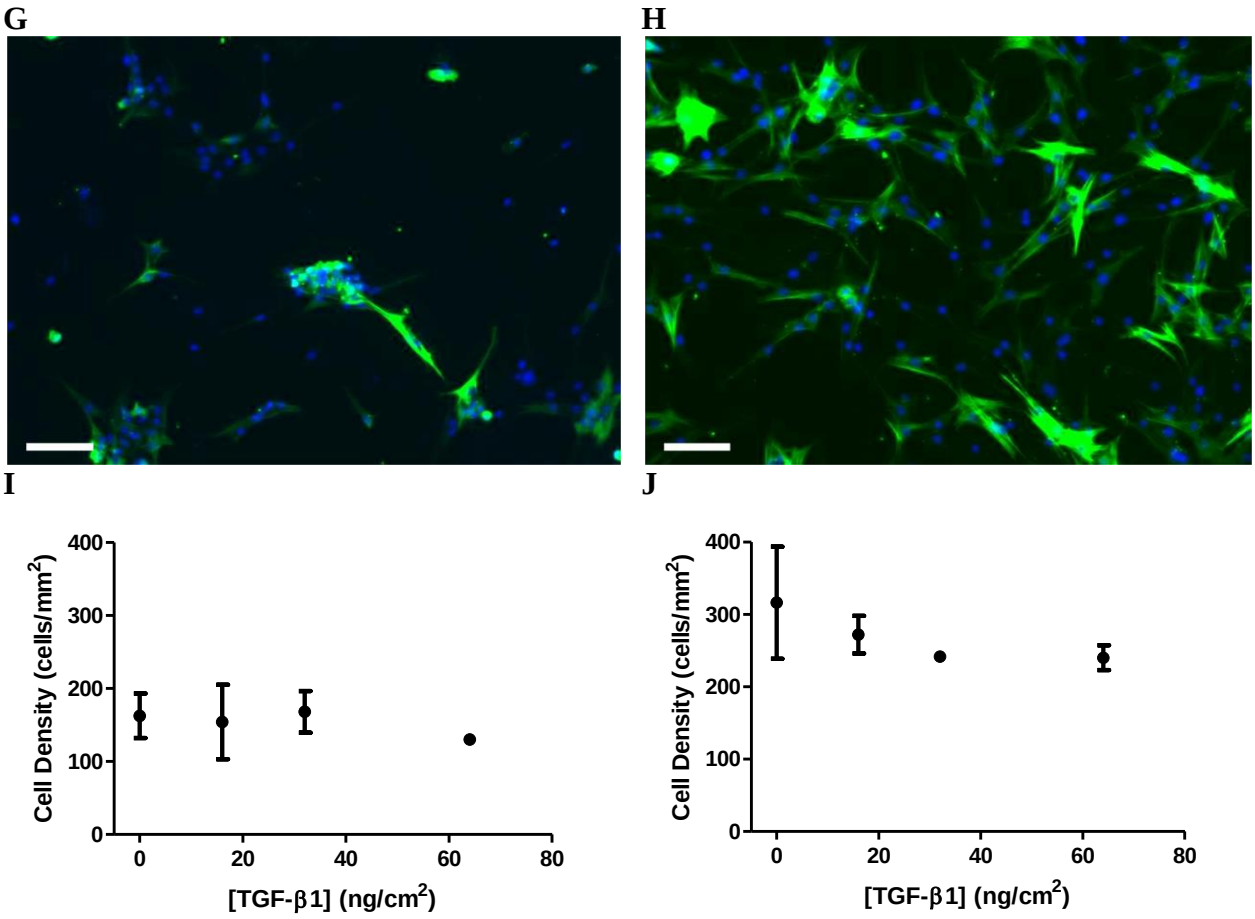

Figure 8 – VIC images of 4 kPa (A, C, E, G) and 21 kPa (B, D, F, H) hydrogels taken at lower magnification than Figures 6 and 7 to illustrate cell density. Hydrogels were conjugated with 64 ng/cm^2 (A, B), 32 ng/cm^2 (C, D), 16 ng/cm^2, (E, F), and 0 ng/cm^2 (G, H) TGF-β1. Scale bar represents 100 μm. I) and J) show plots of cell density versus TGF-β1 surface density of 4 kPa and 21 kPa hydrogels respectively. Error bars represent standard error of the mean, and each condition was done in triplicate.

To assess VIC adhesion to the various hydrogel conditions, the average cell density was calculated for each condition by counting the number of DAPI stained nuclei and dividing by the frame area (Fig. 8). For the 4 kPa conditions, cell density remained relatively constant over all TGF-β1 surface concentrations. For the 21 kPa conditions, cell density exhibited a decreasing trend from the lowest TGF-β1 surface concentration to the highest surface concentration. However, there was a significant amount of fluctuation in some of the conditions. When directly compared, the 21 kPa conditions had higher cell densities at each surface concentration of TGF-β1 than did the 4 kPa conditions. Furthermore, VICs on all 21 kPa conditions exhibited greater spread morphologies on the hydrogels compared to VICs on the 4 kPa conditions. A majority of VICs on the softer substrates exhibited rounded morphologies and tended to cluster together possibly indicating that the VICs favored cell-cell adhesions over cell-matrix adhesions. This clustering occurred at all surface concentrations of TGF-β1 on the 4 kPa hydrogels.

In a separate experiment, VICs were seeded on 16 kPa hydrogels with 0, 16, 32, and 64 ng/cm^2 TGF-β1 surface concentrations and allowed to incubate for 36 hours before being imaged (Fig. 9). On all replicates for the 32 and 64 ng/cm^2 TGF-β1 surface concentrations, VIC nodules were observed. However, on all replicates for the 0 and 16 ng/cm^2 TGF-β1 surface concentrations, no VIC nodules were observed. While this modulus is less than the moduli used in the other cell experiments, it is still greater than the 15 kPa activation threshold for VICs, and thus, these results were used in comparison to the stiff modulus conditions in Fig. 6 and 7.

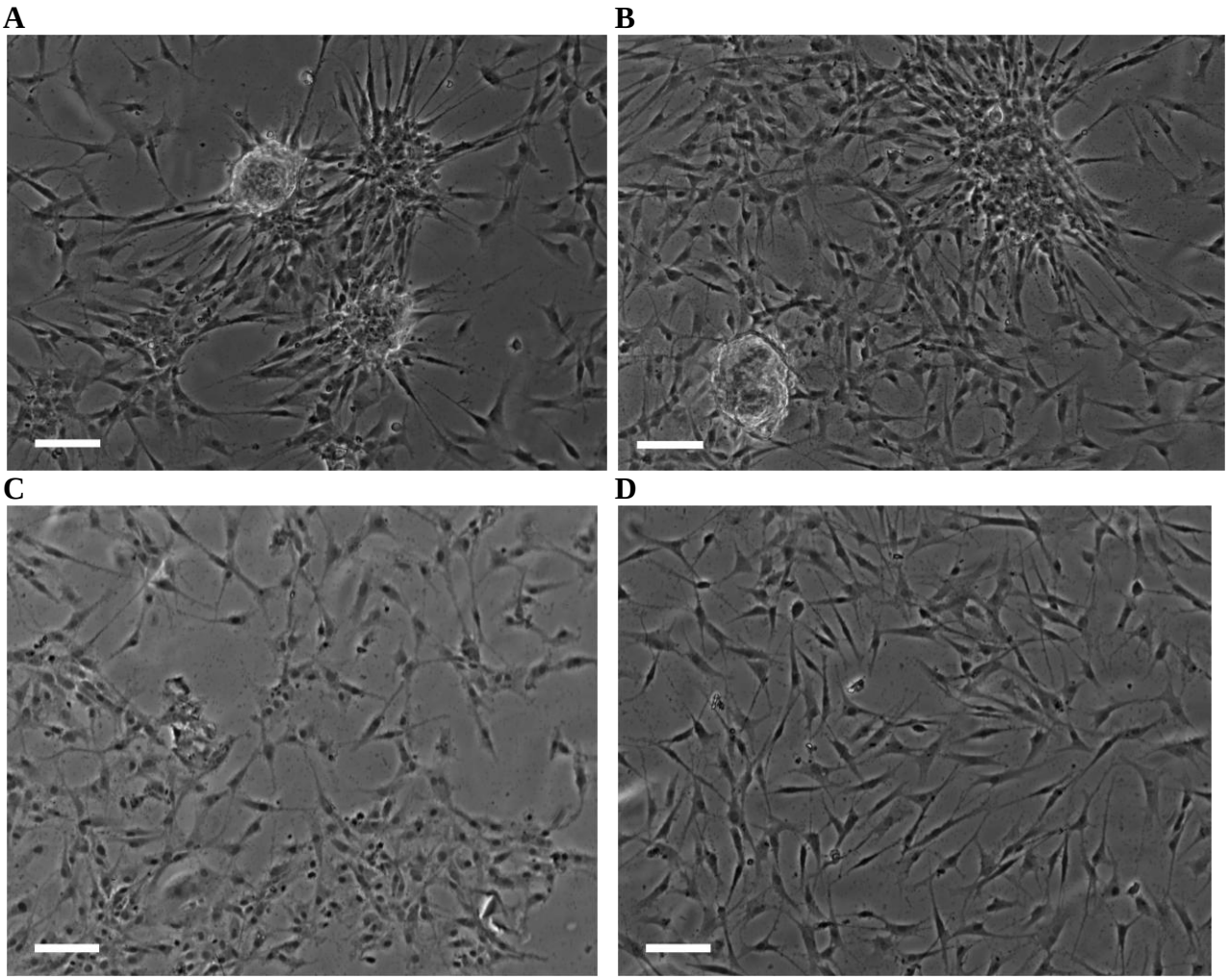

Figure 9 – Bright field images of VIC nodule formation on 16 kPa hydrogels at different surface concentrations of TGF-β1: A) 64 ng/cm^2, B) 32 ng/cm^2, C) 16 ng/cm^2, and D) 0 ng/cm^2. Cells were seeded at 30,000 cells/cm^2 and imaged after 36 hours. Scale bar represents 100 μm. All conditions performed in triplicate. Note nodule formation in A) and B), but not in C) and D).

Discussion

In this study, 4-arm PEG-norbornene hydrogels were used to investigate the effect of TGF-β1 and environmental modulus on the behavior of VICs. To do this, thiolated TGF-β1 was conjugated to the surface of off-stoichiometric hydrogels through thiol-ene photochemistry with excess unreacted norbornene present in the hydrogel. The presence and bioactivity of conjugated TGF-β1 was confirmed via ELISA and luciferase reporter gene assay with a mink lung epithelial cell line, respectively. By controlling the concentration of TGF-β1 added to the hydrogel surface, both ELISA and luciferase signals were increased (Figs. 2 and 3). Furthermore, changing the PEG weight percent in the monomer solution provided a facile method for tailoring the stiffness of these hydrogels (Fig. 4). From these results, approximate surface concentrations of bioactive TGF-β1 can be controlled over a range of 0 – 84 ng/cm^2 and hydrogel Young's modulus can be controlled over a range of 4 – 21 kPa.

Generally, cells seeded on soft materials exhibit a more rounded phenotype, have fewer focal adhesions, experience growth arrest, and are more prone to apoptosis than compared to cells seeded on stiffer materials (Wells, 2008). Some of these characteristics were directly observed in this study. VICs seeded on low modulus hydrogel (~4 kPa) had a much more rounded phenotype than VICs seeded on high modulus (~21 kPa) material. This discrepancy is likely a consequence of less tension within the actin-myosin cytoskeleton when cells exert a force on the softer hydrogel surface, leading to a more rounded morphology. Furthermore, the VICs may then depend more on cell-cell interactions through transmembrane receptors, such as cadherins, to regulate their cytoskeletal tension. As was seen on all 4 kPa conditions, this cell-cell interaction preference leads to the clustering of VICs (see Fig. 8A, C, E, G).

Interestingly, VICs seeded on softer modulus conditions did not respond as dramatically to the presence of tethered TGF-β1 as the VICs seeded on the stiffer modulus (Fig. 6E and 7E). Furthermore, cells exhibited a wide variability of activation responses within each condition (see Fig. 6E). This could be due to the importance of the actin-myosin framework in multiple cellular processes. VICs seeded on softer substrates exhibit less αSMA organization than on stiffer substrates. Because the actin-myosin cytoskeletal network is responsible for transportation of vesicles across the cell and involved in some signal transductions, this lack of actin organization can interrupt these processes with potential increases in cell death (Van de Water, 1996; Gourlay, 2004; Thomas, 2006). However, further cellular characterizations would be needed to confidently conclude this. For example, conducting qRT-PCR of αSMA levels would help understanding of how intracellular αSMA concentrations change in each experimental condition; further, measuring caspase 3/7 activity could characterize the level of apoptotic signaling occurring in each experimental condition.

VICs seeded on the stiffer modulus substrate expressed a different behavior than those seeded on the softer substrate. On the stiffer substrate, VICs exhibited a more spread morphology, qualitatively higher levels of αSMA expression, and a different trend to varying surface concentrations of TGF-β1. From the 0 ng/cm^2 to 16 ng/cm^2 conditions, the VIC activation increased, as a higher percentage of cells had αSMA stress fibers. Interestingly, this trend did not extend to higher surface TGF-β1 concentrations, as there was significant drop ($p < 0.01$) in activation between the 16 ng/cm^2 and 32 ng/cm^2 TGF-β1 surface concentration conditions. This abrupt change in activation correlates well with the development of VIC nodules (Fig. 9). When progressing to a diseased phenotype, VICs form nodules, up-regulate calcification associated proteins, and apoptose (Jian et al., 2003; Freeman, 2005; Liu et al., 2007). This

induced apoptosis should, then, lead to a drop in activation percentage, and these results suggest that a surface concentration threshold exists between 16 ng/cm^2 and 32 ng/cm^2 TGF-β1 conditions. Below this threshold, VICs remain activated and in a myofibroblastic phenotype, while at higher surface concentrations, cells progress to a disease state, form nodules, and apoptose. This conclusion can be further supported by the qualitative drop in cell density observed on the stiffer modulus condition (although not statistically significant), possibly suggesting a TGF-β1-mediated apoptosis mechanism.

To confirm these conclusions, further cellular characterizations are needed. As previously described, VIC activation can also be characterized by measuring αSMA mRNA levels using qRT-PCR, and while measuring caspase 3/7 activity levels can be used to quantify apoptosis in each experimental condition. In assessing VIC progression to a diseased phenotype, a number of proteins are up-regulated, including BMP-2, osteopontin, and osteocalcin. Assays for each of these proteins could be used to determine which modulus and TGF-β1 surface concentration conditions activate VICs to an osteoblastic phenotype. Finally, VIC nodule formation is dependent on alkaline phosphatase activity (Mathieu et al., 2005); thus, measuring alkaline phosphatase activity may help determine experimental conditions implicated in leading VICs to progress to an osteoblastic phenotype.

Conclusion

In this study, PEG-norbornene hydrogels were used to assess the effects of environmental modulus and TGF-β1 surface concentration on the behavior of valvular interstitial cells. PEG hydrogels with 0, 16, 32, and 64 ng/cm^2 TGF-β1 surface densities were synthesized, and TGF-β1 was detectable via both immunodetection and bioactivity assays. Furthermore, stiffness of the gel platform could be varied by changing the weight percent of PEG monomer. When VICs were seeded on the surface of these materials, the cells showed little adherence to the 4 kPa hydrogels, resulting in decreased cell density and a lack of response to tethered TGF-β1. VICs seeded on 21 kPa hydrogels, however, exhibited greater adherence and spread morphology. Furthermore, from both activation and nodule formation trends, a TGF-β1 threshold concentration may exist between 16 ng/cm^2 and 32 ng/cm^2, below which VICs remain an activated myofibroblast phenotype, and above which VICs progress to potentially a diseased phenotype, form nodules, and apoptose.

Acknowledgements

I would like to thank Dr. Kristi Anseth for her mentorship and guidance on this project as well as throughout most of my undergraduate career. I am incredibly grateful for the opportunities she has given me through working in her lab, and I have definitely grown both personally as well as in my capacity as a scientist. I am lucky to have been able to work with such a gifted scientist, and I am confident these skills and experiences will greatly benefit me in my future medical endeavors. I would also like to thank Dr. Leslie Leinwand for her sponsorship in completing an Honors Thesis as well as for her guidance throughout the project.

Throughout the course of this project, I was mentored on a day-to-day basis by Chemical and Biological Engineering Ph.D student Joshua McCall. His assistance in experimental design, troubleshooting, data analysis, and manuscript editing were invaluable, and I am incredibly grateful to him for taking me on as an Honors Thesis student. I wish him the best of luck in his future endeavors. I would also like to thank Sharon Wang, Ph.D student in Molecular, Cellular, and Developmental Biology. Her assistance and guidance on the cellular applications of this project were likewise invaluable, and I am very grateful for all of her mentoring. Finally, I would like to extend my appreciation to Dr. Julie Benton, Dr. April Kloxin, Dr. Sarah Anderson, Dr. Patrick Hume, Dr. Ben Fairbanks and Ph.D students Cole DeForest, Sarah Trexler, and Abby Bernard, as well as all other past and present Anseth Research Group members with whom I interacted and received assistance. I wish you all the best of luck in your future endeavors.

This work was funded through NIH grant AR053126 and the Howard Hughes Medical Institute (HHMI) and conducted in Dr. Kristi Anseth's laboratory. Student stipend was graciously funded by the Undergraduate Research Opportunities Program/HHMI Biosociences Research Grant.

References

Benton JA, Kern HB, Leinwand LA, Mariner PD, Anseth KS. (2009). Statins block calcific nodule formation of valvular interstitial cells by inhibiting alpha-smooth muscle actin expression. *Arteriosclerosis, Thrombosis, and Vascular Biology*. 29: 1950-57.

Benton JA, Fairbanks BD, Anseth KS. (2010). Characterization of valvular interstitial cell function in three dimensional matrix metalloproteinase degradable PEG hydrogels. *Biomaterials*. 30: 6593-6603.

Bershadsky A, Kozlov M, Geiger B. (2006). Adhesion-mediated mechanosensitivity: a time to experiment, and a time to theorize. *Curr Opin Cell Biol.*18:472-481.

Butcher JT, Mahler GJ, Hockaday LA. (2011). Aortic valve disease and treatment: The need for naturally engineered solutions. *Adv Drug Del Rev.* Accepted. In press. doi: 10.1016/j.addr.2011.01.008

Chou CH, Cheng WTK, Lin CC, Chang CH, Tsai CC, Lin FH. (2005). TGF-β1 Immobilized Tri-co-polymer for Articular Cartilage Tissue Engineering. *Wiley Interscience*. In press. doi: 10.1002/jbm.b. 30432

Clark CC, Brown ML, Erickson RA, Shi Y, Liu X. (2009). Transforming Growth Factor β Depletion Is The Primary Determinant of Smad Signaling Kinetics. *Mol Cell Bio,* 29(9): 2443-55.

Cushing MC, Liao JT, Anseth KS. (2005). Activation of valvular interstitial cells is mediated by transforming growth factor-beta1 interactions with matrix molecules. *Matrix Biol.* (24): 428–437

Darby I, Saklli O, Gabbiani G. (1990). α-Smooth muscle actin is transiently expressed by myofibroblasts during experimental wound healing. *Lab. Invest.* 63: 21-29.

Desmouliere A, Badid C, Bochaton-Piallat ML, Gabbiani G. (1997). Apoptosis during wound healing, fibrocontractive diseases and vascular wall injury. *Int J Biochem Cell Biol.* (29): 19–30

El-Hamamsy I, Balachandran K, Yacoub MH, Stevens LM, Sarathchandra P, Taylor PM, Yoganathan AP, Chester AH. (2008). Endothelial-Dependent regulation of the mechanical properties of aortic valve cusps. *J Amer Col Car Foun.* 53(16): 1448-55.

Engler AJ, Sen S, Sweeney HL, Discher DE. (2006). Matrix elasticity directs stem cell lineage specification. *Cell* 126: 677–689.

Fairbanks BD, Schwartz MP, Halevi AE, Nuttelman CR, Bowman CN, Anseth KS. (2009). A Versatile Synthetic Extracellular Matrix Mimic via Thiol-Norbornene Photopolymerization. *Advanced Materials.* 21: 5005-10.

Fairbanks BD, Schwartz MP, Bowman CN, Anseth KS. (2009). Photoinitiated polymerization of PEG-diacrylate with lithium phenyl-2,4,6-trimethylbenzoylphosphinate: polymerization rate and cytocompatibility. *Biomaterials*. 30(35): 6702-6707.

Fan VH, Au A, Tamama K, Littrell R, Richardson LB, Wright JW, Wells A, Griffith LG. (2007). Tethered epidermal growth factor provides a survival advantage to mesenchymal stem cells. *Stem Cells*. 25: 1241–1251.

Ferdous Z, Jo H, Nerem RM. (2011). Differences in valvular and vascular cell response to strain in osteogenic media. *Biomaterials*. In press. doi:10.1016/j.biomaterials.2011.01.030

Freeman RV, Otto CM. (2005). Spectrum of Calcific Aortic Valve Disease. *Circulation*. 111: 3316-26.

Gilbert PM, Havenstrite KL, Magnusson KEG, Sacco A, Leonardi NA, Kraft P, Nguyen NK, Thrun S, Lutholf MP, Blau HM. (2010). Substrate Elasticity Regulates Skeletal Muscle Stem Cell Self-Renewal in Culture. *Science*. 329: 1078-81.

Gourlay CW, Carpp LN, Timpson P, Winder SJ, Ayscough KR. (2004). A role for the actin cytoskeleton in cell death and aging in yeast. *J Cell Biol*. 164(6): 803-9.

Hinz, B. (2007). Formation and function of the myofibroblast during tissue repair. *J Invest Derm.* 127: 526 – 537

Hua, X., X. Liu, D. O. Ansari, and H. F. Lodish. (1998). Synergistic cooperation of TFE3 and smad proteins in TGF-β-induced transcription of the plasminogen activator inhibitor-1 gene. *Genes Dev*. 12:3084–3095.

Hume PS & Anseth KS. (2009). Inducing local T cell apoptosis with anti-Fas-functionalized polymeric coatings fabricated via surface-initiated photopolymerizations. *Biomaterials.* 31(12): 3166-74.

Ingber DE. (2006). Cellular mechanotransduction: putting all the pieces together again. *FASEB J.* 20:811-827.

Jian B, Navneet N, Li Q, Mohler ER, Levy RJ. (2003). Progression of aortic valve stenosis: TGF-β1 is present in calcified aortic valve cusps and promotes aortic valve interstitial cell calcification via apoptosis. *Ann Thoracic Surg*. 75: 457-66

Kaden JJ, Dempfle CE, Grobholz R, Tran HT, Kilic R, Sarikoc A, Brueckmann M, Vahl C, Hagl S, Haase KK, Borggrefe M. (2003). Interleukin-1 beta promotes matrix metalloproteinase expression and cell proliferation in calcific aortic valve stenosis. *Atherosclerosis*. 170: 205–211.

Kloxin AM, Benton JA, Anseth KS. (2010). *In situ* elasticity modulation with dynamic substrates to direct cell phenotype. *Biomaterials*. 31: 1-8.

Li Z, Dranoff JA, Chan EP, Uemura M, Sevigny J, Wells RG. (2007). Transforming growth factor-beta and substrate stiffness regulate portal fibroblast activation in culture. *Hepatology.* 46(4): 1246-56.

Liu AC, Joag VR, Gotlieb AR. (2007). The Emerging Role of Valve Interstitial Cell Phenotypes in Regulating Heart Valve Pathobiology. *Am Jour Path.* 171(5): 1407-18.

Lutolf MP, Gilbert PM, Blau HM. (2009). Designing materials to direct stem-cell fate. *Nature*. 462(26): 433-441.

Mann BK, Schmedlen RH, West JL. (2000). Tethered-TGF-β increases extracellular matrix production of vascular smooth muscle cells. *Biomaterials*. 22: 439-44.

Mathieu P, Voisine P, Pepin A, Shetty R, Savard N, Dagenais F. (2005). Calcification of human valve interstitial cells is dependent on alkaline phosphatase activity. *J Heart Valve Dis.* 14 :353–357

Mohler III ER, Chawla MK, Chang AW, Vyavahare N, Levy RJ, Graham L, Gannon FH. (1999). Identification and characterization of calcifying valve cells from human and canine aortic valves. *J Heart Valve Dis.* 8: 254–260

Nur-E-Kamal A, Ahmed I, Kamal J, Babu AN, Schindler M, Meiners S. (2008). Covalently attached FGF-2 to three-dimensional polyamide nanofibrillar surfaces demonstrates enhanced biological stability and activity. *Mol. Cell. Biochem*. 309: 157–166.

Otto CM, Kuusisto J, Reichenbach DD, Gown AM, O'Brien KD. (1994). Characterization of the early lesion in "degenerative" valvular aortic stenosis: histological and immunohistochemical studies. *Circulation*. 90: 844–853.

Ruoslahti E. (1996). RGD and other recognition sequences for integrins. *Ann Rev Cell Dev Bio.* 12: 697–715.

Simmons CA, Grant GR, Manduchi E, Davies PF. (2005). Spatial heterogeneity of endothelial phenotypes correlates with side-specific vulnerability to calcification in normal porcine aortic valves. *Circ Res*. 96(7): 792-9.

Thomas SG, Huang S, Li S, Staiger CJ, Franklin-Tong VE. (2006). Actin depolymerization is sufficient to induce programmed cell death in self-compatible pollen. *J Cell Biol.* 174(2): 221-229.

Thubrikar M, Piepgrass WC, Deck JD, Nolan SP. (1980). Stresses of natural versus prosthetic aortic valve leaflets in vivo. *Ann Thor Surg*. 30(3): 230-239

Tomasek JJ, Gabbiani G, Hinz B, Chaponnier C, Brown RA. (2002). Myofibroblasts and mechano-regulation of connective tissue remodeling. *Nat Rev Mol Cell Biol.* 3: 349-63.

Van de Water B, Kruidering M, Nagelkerte JF. (1996). F-actin disorganization in apoptotic cell death of cultured rat renal proximal tubular cells. *Amer J Phys Renal Phys.* 270(4): F593-F603.

Walker GA, Masters KS, Shah DN, Anseth KS, Leinwand LA. (2004). Valvular myofibroblast activation by transforming growth factor-β: implications for pathological extracellular matrix remodeling in heart valve disease. *Circ Res.* (95): 253–260

Warren BA, Yong JLC. (1997). Calcification of the aortic valve: its progression and grading. *Pathology*. (29): 360 –368.

Wells RG. (2008). The role of matrix stiffness in regulating cell behavior. *Hepatology*. 47(4): 1394-1400.

Yoshioka M, et al. (2006). Chondromodulin-I maintains cardiac valvular function by preventing angiogenesis. *Nat Med*. 12(10): 1151-59